ACS SENSORS

pubs.acs.org/acssensors

Article

Nanoporous Anodic Alumina-Based Sensor for miR-99a-5p Detection as an Effective Early Breast Cancer Diagnostic Tool

Iris Garrido-Cano, Luis Pla, Sara Santiago-Felipe,* Soraya Simón, Belen Ortega, Begoña Bermejo, Ana Lluch, Juan Miguel Cejalvo, Pilar Eroles, and Ramón Martínez-Máñez*

Cite This: *ACS Sens.* 2021, 6, 1022−1029

Read Online

ACCESS | Metrics & More | Article Recommendations

ABSTRACT: Circulating microRNAs have emerged as potential diagnostic biomarkers. The deregulation of the microRNA miR-99a-5p has been previously described as an effective biomarker of early breast cancer. Herein, we present a new nanoporous anodic alumina (NAA)-based biosensor that can detect plasma miR-99a-5p with high sensitivity and selectivity. NAA pores are loaded with rhodamine B and capped with a specific oligonucleotide that is able to block cargo release until the target is present. In the presence of miR-99a-5p, the capping oligonucleotide recognizes the miR-99a-5p sequence and displaces it allowing the release of the encapsulated dye. This method is able to successfully distinguish healthy controls from breast cancer patients, even at early stages with high efficiency, showing the presented system as a promising tool for breast cancer detection.

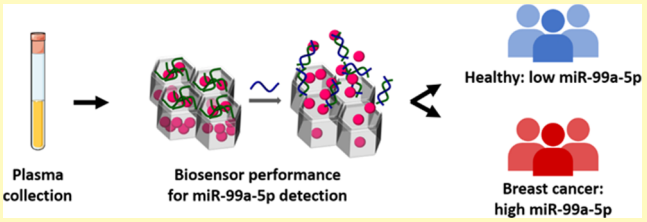

KEYWORDS: *breast cancer, plasma, diagnosis, nanoporous anodic alumina, biosensor*

Breast cancer (BC) is one of the most common types of cancer in the world and one of the leading causes of cancer-related death in women.[1] Early BC diagnosis has been proven to significantly improve the patient's survival rates. The five-year survival rate for BC patients diagnosed at stage I is 98% and falls until 25% for those diagnosed at stage IV.[2−4] Currently, mammography is the gold-standard technique for diagnosis, but it presents some limitations such as radiation exposure, as well as low sensitivity and specificity in young women with dense breast tissue.[5] Therefore, the development of new diagnostic tools for early BC detection is needed.

Interest in microRNAs (miRNAs) has recently emerged due to their potential application as diagnostic biomarkers.[3,6,7] They consist of small noncoding ribonucleic acids (RNAs) of 19−25 nucleotides that regulate gene expression through different mechanisms.[8] Their deregulation has been described in many diseases including BC, where they have been associated with tumor aggressiveness, prognosis, response to treatment, and clinical outcome.[6,9−11] Indeed, several authors evidenced the relevance of circulating miRNAs in plasma as minimally invasive biomarkers for the prognosis and diagnosis of different types of cancers.[7,12,13] Nowadays, the detection of circulating miRNAs is mainly assessed in laboratories through quantitative real-time PCR (qRT-PCR), microarrays, northern blotting, and RNA sequencing, which are time-consuming and complex techniques. As a result, the detection of miRNAs as a diagnosis tool falls outside the clinical context.

Implementing circulating miRNAs for diagnosis requires the development of effective, rapid, simple, and low-cost analytical methods. In this context, nanomaterials and, in particular, nanoporous anodic alumina (NAA), have emerged as optimal supports for the design of several biosensors for numerous sensing applications.[14] To provide specificity, nanoporous entrances are blocked with molecular gates (also known as gatekeepers or nanovalves) of different nature (such as proteins, enzymes, antibodies, metallic nanoparticles, organic molecules, polymeric structures, and deoxyribonucleic acid (DNA) sequences) that can control cargo delivery depending on the presence or absence of a stimulus.[15−17] In these systems, NAA was loaded with a chromo-fluorogenic reporter and capped with selective molecules that are able to recognize a specific analyte. Therefore, the dye remains inside the pores until capping molecules recognize the target (bio)molecule, triggering its displacement and inducing payload release. Based on this approach, it is possible to detect cations, anions, and biomolecules.[18−24] As a particularity of this sensing concept, host−guest interaction is independent of the signaling subunit and, besides, an amplifying effect is provided since few stimuli

Received: October 23, 2020
Accepted: January 22, 2021
Published: February 18, 2021

https://dx.doi.org/10.1021/acssensors.0c02222
ACS Sens. 2021, 6, 1022−1029

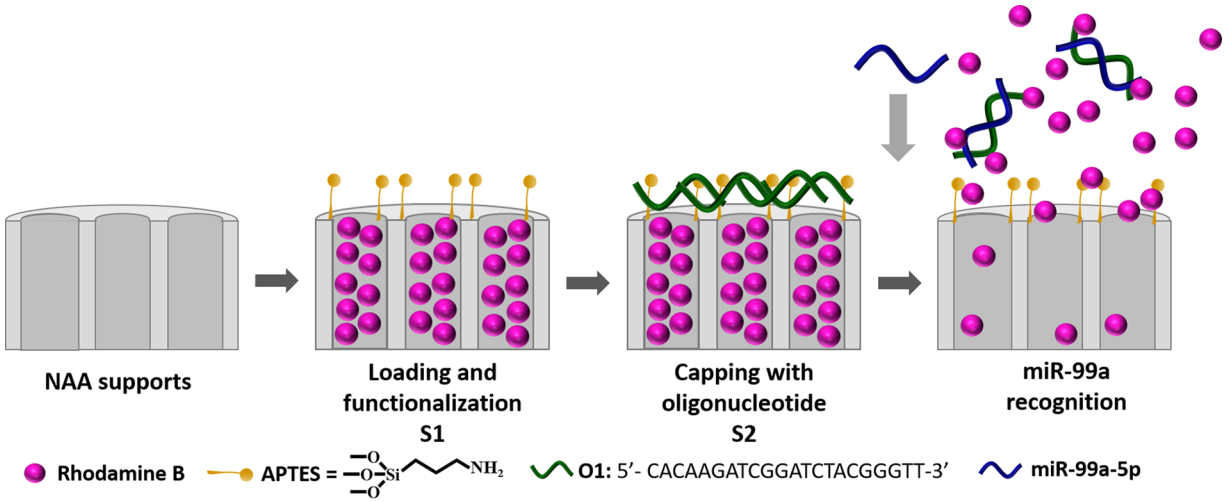

Figure 1. Schematic representation of the preparation and sensing process of S2 material. Nanoporous anodic alumina (NAA) support was loaded with rhodamine B and functionalized with APTES to obtain solid S1. Solid S2 was obtained after capping with an oligonucleotide with binding affinity for miR-99a-5p. Delivery of the entrapped rhodamine B is selectively achieved in the presence of miR-99a-5p with high-signal amplification.

units are able to release a large quantity of entrapped signaling molecules.

Herein, we present a new DNA-gated mesoporous biosensor for the detection of circulating miR-99a-5p, which has been previously described as an effective biomarker for BC.[25] Our proposed system is based on NAA supports whose pores are loaded with rhodamine B and capped with an oligonucleotide that specifically hybridizes with the miR-99a-5p sequence. Therefore, in the absence of the target miRNA, the capping oligonucleotide continues blocking the pores, inhibiting the dye release. In contrast, in the presence of the miR-99a-5p, there is a favorable DNA−RNA interaction between the microRNA and the capping oligonucleotide that induces the uncapping of the pores, giving rise to dye delivery. High selectivity and sensibility were accomplished, and, after confirming the potential of our system in vitro, its diagnosis applicability was validated in plasmas from healthy controls and BC patients.

EXPERIMENTAL SECTION

General Techniques. Field emission scanning electron microscopy (FESEM) experiments, including energy-dispersive X-ray spectroscopy (EDX), were performed on a ZEISS Ultra 55 microscope. Fluorescence spectra were measured on a microplate reader (Synergy H1, BioTek, Winooski, VT).

Chemicals. (3-Aminopropyl)triethoxysilane (APTES), hydrochloric acid, rhodamine B, and tris(hydroxymethyl)aminomethane (TRIS) were purchased from Sigma-Aldrich (Spain). NAA supports were provided by InRedox Company (Longmont, CO). O1 sequence 5′-CAC AAG ATC GGA TCT ACG GGT T-3′ was designed as the complementary sequence of miR-99a-5p (obtained from mirbase.org) and was obtained from Thermo Fisher Scientific (Waltham, MA). MiRvana mimics of miRNA-99a-5p, miR-200c-3p, miR-449c-3p, miR-221-3p, miR-21-5p, and the mirVana miRNA Mimic Negative Control no.1 were obtained from Thermo Fisher Scientific (Waltham, MA).

Synthesis of Solids. To prepare S1, NAA supports of 2 mm diameter were immersed in 8 mL of rhodamine B solution in acetonitrile (1 mM, ACN) and stirred for 24 h to ensure its entrance inside the pores. Then, the mesoporous surface was functionalized by the addition of APTES (1.32 mmol, 328 μL) and stirred at room temperature for 6 h. Afterward, the obtained S1 supports were washed dropwise with a rhodamine B-ACN solution and dried overnight at room temperature.

Then, the final solid S2 was obtained by submerging S1 in a solution of the capping oligonucleotide O1 in TRIS hybridization buffer (20 mM Tris−HCl, 37.5 mM $MgCl_2$, pH 7.5). After the corresponding optimization, capping conditions were established in 20 μL of O1 (100 μM) in a 250 μL final volume of TRIS hybridization buffer for two S1 supports agitated at 37 °C during 1 h. Finally, the as-prepared S2 solids were washed with TRIS hybridization buffer to remove the leftover O1.

Cargo Quantification. To determine the quantity of the loaded rhodamine B inside the pores, two S2 supports were immersed in the hybridization buffer (1 mL). Then, one of the supports was stirred for 1 h at 90 °C to induce maximum cargo delivery. As a control, the other support was stirred for 1 h at 25 °C. To quantify the released fluorophore, fluorescence was measured (λ_{exc} = 555 nm, λ_{em} = 575 nm), and the released dye was determined using a calibration curve. The experiment was carried out in triplicate.

Detection Protocol. The S2 ability for recognition and detection of miRNA-99a-5p was determined by fluorescence spectroscopy measurements of the delivered fluorescence indicator entrapped into the nanostructure of the supports in the absence and the presence of the miRNA-99a-5p sequence. In a typical experiment, two different and independent S2 solids were submerged in separate solutions containing 900 μL of TRIS hybridization buffer. Then, 100 μL of miRNA-99a-5p (1 μM) or TRIS hybridization buffer (control) were inoculated into the solids and stirred for 1 h at 37 °C. Aliquots were collected every 15 min. The released rhodamine B was monitored by measuring the fluorescence at 575 nm (λ_{exc} = 555 nm). The experiment was carried out in triplicate.

Amplification Assay. To determine the signal amplification, two S2 solids were immersed in 900 μL of TRIS hybridization buffer. Then, 100 μL of miRNA-99a-5p (1 μM) was added to one support. As a control, 100 μL of the hybridization buffer was added to the second support. Solids were incubated for 1 h at 37 °C, and the released fluorophore was measured at 575 nm (λ_{exc} = 555 nm). Finally, the amount of released dye was determined by using a calibration curve.

Selectivity Assessment. To evaluate the selectivity of the synthesized sensor, seven individual and separate S2 supports were submitted to the presence of target mRNA-99 as well as other miRNA sequences such as miR-200c-3p, miR-449c-3p, miR-221-3p, miR-21-5p, and the mirVana miRNA Mimic Negative Control no. 1, all of them at a final concentration of 10^{-1} μM in 1 mL of TRIS hybridization buffer, and stirred for 1 h at 37 °C. The response to the bare TRIS hybridization buffer was also evaluated as a negative control experiment. The delivered rhodamine B was determined by

https://dx.doi.org/10.1021/acssensors.0c02222
ACS Sens. 2021, 6, 1022−1029

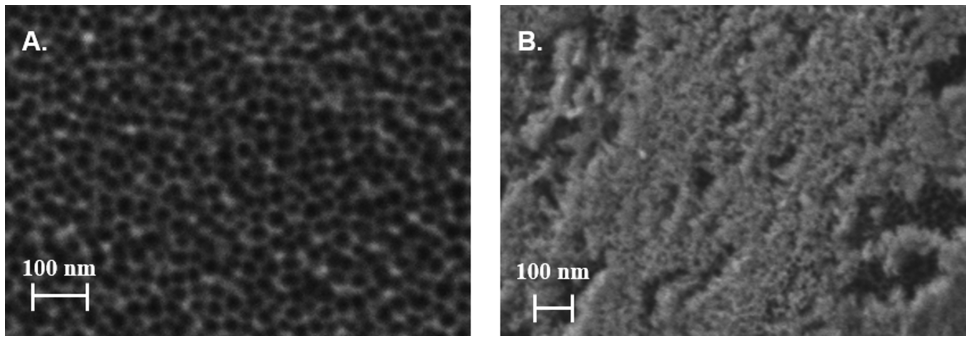

Figure 2. FESEM images of (A) NAA support and (B) S2.

fluorescence (λ_{exc} = 555 nm, λ_{em} = 585 nm). The experiment was carried out in triplicate with an average of 21 S2 supports.

Determination of Sensitivity of miRNA-99a-5p in Real Competitive Media. The response of S2 to decreasing concentrations of miRNA-99a-5p was evaluated in human plasma media. For that, eight S2 materials prepared were separately immersed in 200 μL of plasma from non-BC patients. Then, 200 μL of 10-fold dilutions of miRNA-99a-5p was added to reach a final concentration between 0 and 500 nM. Mixtures were stirred for 60 min at room temperature and aliquots were obtained at 0 and 60 min. Finally, the diffused rhodamine B was determined by fluorescence emission at 575 nm (λ_{exc} = 555 nm). The experiment was carried out in triplicate with an average of 24 S2 supports.

Validation in Clinical Samples. Plasma samples from 47 BC patients were collected before treatment from Biomedical Research Institute INCLIVA (Spain). Plasma samples from 47 healthy volunteers were obtained from the same institution and the Valencian Biobanking Network. Ethylenediaminetetraacetic acid (EDTA)-containing blood tubes were centrifuged at 2000 rpm for 10 min at 4 °C. The superior phase corresponding to the plasma was stored at −80 °C until further use.

To carry out the validation analysis, 250 μL of plasma was added to S2 supports and diluted in 150 μL of TRIS hybridization buffer (final assay volume, 400 μL). Supports were stirred for 1 h at 37 °C. Then, fluorescence emission was measured at 575 nm (λ_{exc} = 555 nm) at 0 and 60 min to determine the amount of diffused rhodamine B. TRIS buffer was used as a negative control.

Ethical Committee. Informed consent was obtained from all subjects included in this work, and the study was approved by the Ethics Committee of INCLIVA (2019/196) in accordance with the ethical standards of the Declaration of Helsinki.

Statistical Analysis. Differences between groups were evaluated by Mann−Whitney U or Kruskal Wallis nonparametric tests. The receiver-operating characteristic (ROC) curves were applied to determine the diagnostic value of our nanodevice, and the area under curve (AUC) was calculated. The optimal sensitivity, specificity, and accuracy were obtained according to Youden's J index (sensitivity + specificity − 1).[31,32] Statistical analyses were carried out with GraphPad Prism 6.01 (GraphPad Software). Results were considered statistically significant when *P*-value was <0.05.

RESULTS AND DISCUSSION

Design, Synthesis, and Characterization of the Functional Nanodevice. The aim of this work was to develop an effective, rapid, and easy to handle tool to detect circulating miR-99a-5p in clinical samples. To achieve it, pores of NAA support were loaded with the fluorescent dye rhodamine B. Then, the external surface was functionalized with APTES to obtain S1. Subsequently, oligonucleotide O1, which was designed as a complementary sequence of miR-99a-

Table 1. Atomic Elemental Ratios in the Different Solids Prepared

	C/Al	N/Al	P/Al
S1	2.28	0.38	
S2	0.74	0.49	0.01

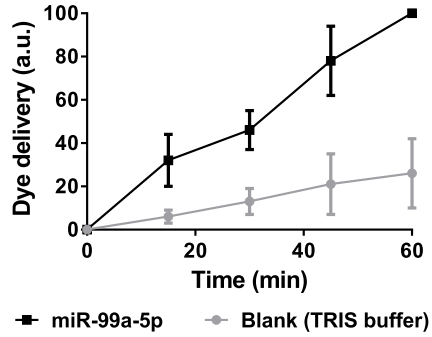

Figure 3. Rhodamine B delivery from the pores of the S2 material in the absence (gray) or in the presence of miR-99a-5p (10^{-1} μM) (black). Mean ± standard deviation (SD).

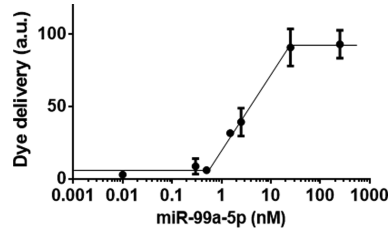

Figure 4. Release of rhodamine B in TRIS buffer (pH 7.4) from support S2 in the presence of different concentrations of miR-99a-5p. Mean ± SD.

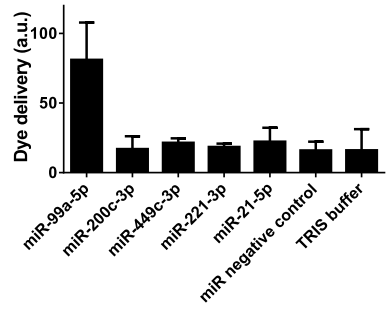

Figure 5. Selectivity of the proposed method. Release of rhodamine B from S2 support in the presence of 10^{-1} μM miR-99a-5p, miR-200c-3p, miR-449c-3p, miR-221-3p, miR-21-5p, miRNA negative control (random sequence), and TRIS buffer. Mean ± SD.

https://dx.doi.org/10.1021/acssensors.0c02222
ACS Sens. 2021, 6, 1022−1029

Table 2. Association between Clinicopathological Features of Breast Cancer Patients and Circulating miR-99a-5p Levels[a]

	number (%)	median (95% CI)	*P* value
histological subtype, *n* (%)			
luminal	29 (61.7%)	11 527 (7318−27 759)	0.444
TNBC	6 (12.8%)	8782 (2457−49 145)	
Her 2-enriched	11 (23.4%)	21 791 (8231−42 082)	
unknown	1 (2.1%)		
grade group, *n* (%)			
1	11 (23.4%)	11 527 (2985−47 462)	0.720
2	23 (48.9%)	19 677 (7605−27 759)	
3	13 (27.6%)	22 562 (7318−42 082)	
stage, *n* (%)			
I	9 (19.1%)	15 768 (7605−42 082)	0.0770
II	25 (53.2%)	8772 (5432−22 735)	
III	8 (17.0%)	22 177 (8792−50 246)	
IV	4 (8.5%)	37 980 (22 479−52 086)	
unknown	1 (2.1%)		
tumor size, *n* (%)			
≤50 mm	40 (85.1%)	11 168 (7933−23 955)	0.3681
>50 mm	5 (10.6%)	22 562 (9164−37 389)	
unknown	2 (4.3%)		
regional lymph node metastasis, *n* (%)			
no	23 (48.9%)	9164 (7605−35 514)	0.8074
yes	22 (46.8%)	17 723 (7933−23 182)	
unknown	2 (4.3%)		
distant metastasis, *n* (%)			
no	42 (89.4%)	11 168 (8231−22 735)	0.85853
yes	4 (8.5%)	29 934 (2457−38 571)	
unknown	1 (2.1%)		

[a]TNBC, triple-negative breast cancer.

5p, was anchored to APTES through electrostatic interactions between positively charged amino moieties provided by APTES functionalization and negative charges from the nucleotide sequence, affording the final S2 sensing material. This system was designed to trigger a specific pore opening in the presence of miR-99a-5p, allowing the delivery of the entrapped rhodamine B (Figure 1).

Characterization of the raw NAA material (S0), S1, and S2 was undertaken by FESEM and EDX analyses. Commercially available NAA supports are composed of a matrix of alumina with funnel-like pores with a diameter that varies between 20 and 30 nm at the top and 5 nm at the bottom, and an average pore density of 9×10^{11} pores·cm^{-2}. The pore profundity reaches ca. 15 nm, and below this depth, the pore configuration becomes uniform along 10 μm. According to the obtained data, this pore morphology allows, approximately, a maximum loading of 4 ng of rhodamine B per μg of NAA. FESEM images of the NAA scaffold and the S2 solid confirmed the porous structure and evidenced structure maintenance after subsequent chemical processes required for system preparation (Figure 2).

The organic content of the successive prepared materials (S0, S1, and S2) was followed by energy-dispersive X-ray spectroscopy (Table 1). High carbon (C/Al: 2.28) and nitrogen (N/Al: 0.38) content was observed in S1 due to the rhodamine B dye loading and APTES functionalization. However, these amounts decreased for S2 because of some unspecific dye leakage during the capping process with O1 and as a result of not complete blockage of the pores. The amount of capping oligonucleotide O1 was evidenced by the presence of phosphorus in the final material S2 (P/Al 0.01) as it was not observed in the NAA support or in S1.

Controlled Delivery Studies. First, in vitro detection of miR-99a-5p was carried out employing our system. In a typical experiment, two separated S2 solids were immersed either in a solution of 10^{-1} μM miRNA in TRIS buffer or in bare TRIS buffer as a control solution. They were incubated for 1 h, and rhodamine B release was determined by fluorescence measurement at selected times. Our results showed that in the absence of miR-99a-5p, dye diffusion from the pores was negligible, with an average dye delivery of less than 20% (Figure 3). In contrast, after the addition of miR-99a-5p, as a result of the complementary hybridization between both miRNA and O1, capping sequences were displaced, pores opened, and dye diffused from the inner structure to the outer solution, as depicted in Figure 1. The observed enhancement in fluorescence emission was attributed to the favorable interaction between the capping oligonucleotide and the miR-99a-5p sequence as well as the intrinsic signal amplification that is observed when gated materials are used. In this context, recent works based on these gated systems have demonstrated that a unique DNA molecule can lead to the delivery of approximately 10^4−10^{11} dye molecules when the pores are opened.[19,20] In this work, it has been determined that 1 nM of miRNA was able to induce the release of an average of 2×10^{11} molecules of rhodamine B, confirming a high-signal amplification capacity.

In a second step, we further evaluated the response of our system to different concentrations of miR-99a-5p. Human plasma solutions containing different spiked concentrations of miRNA were added to several S2 solids, and the dye release was determined after 60 min. We confirmed the correlation between the released rhodamine B and the concentration of miR-99a-5p (Figure 4), which is in agreement with the uncapping protocol, based on the displacement of O1 by complementary hybridization with miR-99a-5p. In these conditions, a linear response in the 0.5−25.0 nM concentration range was observed and a limit of detection (LOD) of 0.5 nM was calculated. It is worth mentioning that this value is in the concentration range of the circulating miRNAs present in the human plasma, which usually varies from femtomolar to nanomolar, suggesting the potential use of the proposed system for the miRNA detection.[26]

In addition, the selectivity of the prepared gated material was tested. For this purpose, we evaluated the response of our system in the presence of 10^{-1} μM miR-200c-3p, miR-449c-3p, miR-221-3p, miR-21-5p, and a miRNA negative control that consists of a random sequence. We compared the dye delivery induced by those biomolecules with the response to miR-99a-5p. After 60 min of incubation, fluorescence emission was

https://dx.doi.org/10.1021/acssensors.0c02222
ACS Sens. 2021, 6, 1022−1029

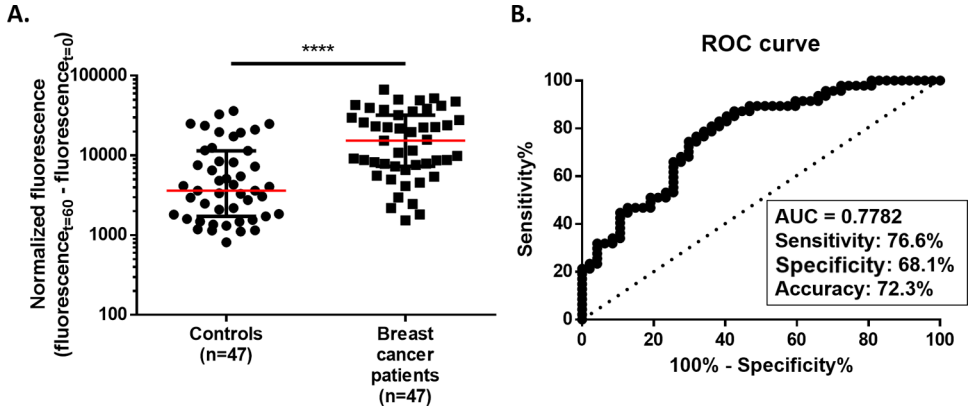

Figure 6. Measurement of miR-99a-5p in human plasma. (A) Expression levels were significantly lower in healthy controls (n = 47) than in breast cancer patients (n = 47). Median (red) ± interquartile range. Mann−Whitney U, ****p < 0.0001. (B) The receiver-operating characteristic (ROC) analysis displays the specificity and sensitivity of the developed sensor to discriminate between breast cancer patients and healthy controls.

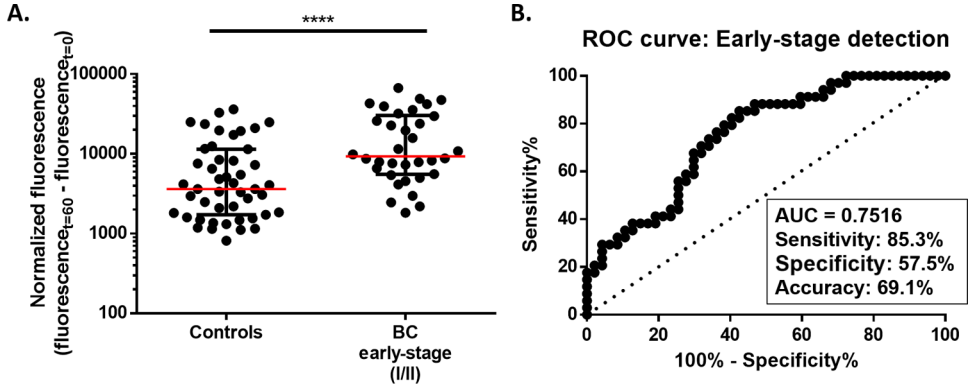

Figure 7. (A) Expression of miR-99a in healthy controls (n = 47) and early-stage breast cancer (BC) (n = 34). Median (red) ± interquartile range. Mann−Whitney U, ****p < 0.0001. (B) The receiver-operating characteristic (ROC) analysis displays the specificity and sensitivity of the developed sensor to discriminate between early-stage BC patients and healthy controls.

determined for each one of the tests. The results indicated that the diffusion of rhodamine B in the presence of other miRNAs was similar to the cargo release in the bare TRIS buffer (Figure 5). By contrast, in the presence of the specific miR-99a-5p sequence, support S2 induced a significant cargo delivery. These results demonstrate that S2 selectively recognizes the miR-99a-5p sequence.

Validation in Clinical Samples. Next, encouraged by the promising results previously obtained, we proceeded to validate the applicability of the nanodevices in real clinical samples. For this purpose, miR-99a-5p was assessed in plasma from 47 healthy controls and 47 BC patients (Table 2). Our results revealed that the levels of released rhodamine B were significantly higher in patients than in healthy controls. The median was 15343 (95% CI, 8706−23182) and 3629 (95% CI, 2487−6495) (p < 0.0001), respectively (Figure 6A). These results clearly agreed with our previous work, where we performed qRT-PCR to determine circulating levels of miR-99a-5p in plasma of BC patients and controls and concluded that miR-99a is overexpressed in plasma from BC patients.[25]

To assess the value of the nanosensor as a diagnostic tool, we computed the ROC curve to discriminate between BC patients and controls. Our system was able to discriminate between BC patients and healthy controls with an AUC of 0.78 (95% CI: 0.69−0.87; p < 0.0001) (Figure 6B). The optimal cut-off value was identified based on the highest value obtained in the ROC curve analysis according to Youden's J index. Using the optimal cut-off value (7285), 76.6% sensitivity, 68.09% specificity, and 72.34% accuracy were obtained. These data provide evidence that the tested nanomaterial may be considered a diagnostic tool for BC.

We also hypothesized that our system could be useful to diagnose BC at a very early stage (stages I and II). We compared the levels of delivered rhodamine B in healthy controls (n = 47) and early-stage BC patients (n = 34). Our data revealed that the levels of released fluorophore were higher in early-stage BC patients (median, 95% CI: 9315, 7318−23955) than in controls (median, 95% CI: 3629, 2487−6495) (Figure 7A). Moreover, our biosensor was able to discriminate between controls and early-stage BC patients with 85.29% sensitivity, 57.45% specificity, and 69.14% accuracy, using the optimal cut-off value of 4426. Nonetheless, AUC was 0.7516 (95% CI: 0.65−0.86; p < 0.0001) for this set of samples (Figure 7B).

Other miRNA biosensors based on different strategies have been developed previously by other authors. Some examples include the system developed by Qavi et al., which was based on photonic resonance in silicon microrings, giving a LOD near 1 nM,[27] or the silver nanocluster DNA probe designed by Yang et al. with a LOD of 20 nM.[28] There is a vast list of different approaches to detect circulating microRNAs, and some authors also validated those systems in biological samples; e.g., Hizir et al. used nanographene oxide for the detection of miR-21 and miR-141 in serum (LOD 1.2 nM)

https://dx.doi.org/10.1021/acssensors.0c02222
ACS Sens. 2021, 6, 1022−1029

and confirmed their detection in some serum samples.[29] Li et al. used hairpin probe-based rolling circle amplification to detect serum miR-486-5p for the diagnosis of lung cancer and tested the system in six healthy controls and six lung cancer patients.[30] Remarkably, to the best of our knowledge, our system is the first NAA-based system designed for the detection of miRNAs. We provided evidence that the proposed method can be performed by directly applying the serum without the involvement of either miRNA isolation or retrotranscription processes, thus being faster than conventional techniques. Moreover, this is a more cost-efficient system, and the required equipment is considered to be of low cost. Besides, the presented strategy may be extrapolated for the development of gated and nanostructured devices for the detection of other circulating miRNAs. Our results evidenced the potential of the presented biosensor for detection of circulating miR-99a-5p as a tool to diagnose early BC. Detection of BC at the initial stages may improve the overall survival. At this moment, the mammography screening programs are proven to decrease disease-specific mortality as well as the occurrence of advanced disease. Furthermore, early detection can result in less radical treatment and less expensive with substantial resource savings.

CONCLUSIONS

Overall, our work provides a promising strategy to diagnose BC patients based on the miR-99a-5p detection in plasma. We have developed a biosensor supported on mesoporous NAA films loaded with rhodamine B and capped with an oligonucleotide that is able to specifically recognize miR-99a-5p. Our results demonstrated that the developed system was able to quantify miRNA expression with high sensitivity and specificity. Moreover, the designed material is simple to prepare, easy to handle, and can discriminate between healthy controls and BC patients, even at very early stages, providing high accuracy. We validated the developed gated system in a total of 94 plasma samples, and our results confirmed that our system might hold great potential for further applications in the clinical diagnosis of BC.

AUTHOR INFORMATION

Corresponding Authors

Sara Santiago-Felipe − *CIBER de Bioingeniería, Biomateriales y Nanomedicina (CIBER-BBN), 28029 Madrid, Spain; Unidad Mixta de Investigación en Nanomedicina y Sensores, Universitat Politècnica de València, Instituto deInvestigación Sanitaria La Fe, 46026 Valencia, Spain; Instituto Interuniversitario de Investigación de Reconocimiento Molecular y Desarrollo Tecnológico (IDM), Universitat Politècnica de València, Universitat de València, 46010 Valencia, Spain;* orcid.org/0000-0002-1731-815X; Email: sasanfe@upvnet.upv.es

Ramón Martínez-Máñez − *CIBER de Bioingeniería, Biomateriales y Nanomedicina (CIBER-BBN), 28029 Madrid, Spain; Unidad Mixta de Investigación en Nanomedicina y Sensores, Universitat Politècnica de València, Instituto deInvestigación Sanitaria La Fe, 46026 Valencia, Spain; Instituto Interuniversitario de Investigación de Reconocimiento Molecular y Desarrollo Tecnológico (IDM), Universitat Politècnica de València, Universitat de València, 46010 Valencia, Spain; Unidad Mixta UPV-CIPF de Investigación en Mecanismos de Enfermedades y Nanomedicina, Universitat Politècnica de València, Centro de Investigación Príncipe, 46012 Valencia, Spain;* orcid.org/0000-0001-5873-9674; Email: rmaez@qim.upv.es

Authors

Iris Garrido-Cano − *Biomedical Research Institute INCLIVA, 46010 Valencia, Spain; CIBER de Bioingeniería, Biomateriales y Nanomedicina (CIBER-BBN), 28029 Madrid, Spain;* orcid.org/0000-0002-1211-473X

Luis Pla − *CIBER de Bioingeniería, Biomateriales y Nanomedicina (CIBER-BBN), 28029 Madrid, Spain; Unidad Mixta de Investigación en Nanomedicina y Sensores, Universitat Politècnica de València, Instituto deInvestigación Sanitaria La Fe, 46026 Valencia, Spain; Instituto Interuniversitario de Investigación de Reconocimiento Molecular y Desarrollo Tecnológico (IDM), Universitat Politècnica de València, Universitat de València, 46010 Valencia, Spain*

Soraya Simón − *Biomedical Research Institute INCLIVA, 46010 Valencia, Spain; Clinical Oncology Department, Hospital Clínico Universitario de Valencia, 46010 Valencia, Spain*

Belen Ortega − *Biomedical Research Institute INCLIVA, 46010 Valencia, Spain; Clinical Oncology Department, Hospital Clínico Universitario de Valencia, 46010 Valencia, Spain*

Begoña Bermejo − *Biomedical Research Institute INCLIVA, 46010 Valencia, Spain; Clinical Oncology Department, Hospital Clínico Universitario de Valencia, 46010 Valencia, Spain*

Ana Lluch − *Biomedical Research Institute INCLIVA, 46010 Valencia, Spain; Clinical Oncology Department, Hospital Clínico Universitario de Valencia, 46010 Valencia, Spain; Centro de Investigación Biomédica en Red de Cáncer (CIBERONC), 46010 Valencia, Spain; Universitat de València, 46010 Valencia, Spain*

Juan Miguel Cejalvo − *Biomedical Research Institute INCLIVA, 46010 Valencia, Spain; Clinical Oncology Department, Hospital Clínico Universitario de Valencia, 46010 Valencia, Spain; Centro de Investigación Biomédica en Red de Cáncer (CIBERONC), 46010 Valencia, Spain*

Pilar Eroles − *Biomedical Research Institute INCLIVA, 46010 Valencia, Spain; Centro de Investigación Biomédica en Red de Cáncer (CIBERONC), 46010 Valencia, Spain; COST Action CA15204, 1210 Brussels, Belgium*

Complete contact information is available at: https://pubs.acs.org/10.1021/acssensors.0c02222

Author Contributions

I.G.-C. and L.P. contributed equally. Conceptualization, I.G.-C., L.P., and S.S.-F; methodology, L.P. and S.S.-F.; validation, I.G.-C., L.P., and S.S.-F.; formal analysis, I.G.-C., L.P., and S.S.-F.; investigation, I.G.-C., L.P., S.S.-F., S.S., B.O., and B.B.; resources, J.M.C., P.E., and R.M.-M.; writing—original draft preparation, I.G.-C. and L.P.; writing—review and editing, S.S.-F, A.L., J.M.C., P.E., and R.M.-M.; supervision, S.S.-F.; project administration, S.S.-F, J.M.C., P.E., and R.M.-M; funding acquisition, R.M.-M. All authors have read and agreed to the published version of the manuscript. All authors have given approval to the final version of the manuscript.

Funding

This work was supported by CIBERONC (CB16/12/00481), CIBER-BBN (CB07/01/2012), Spanish Government PI18/01219 (ISCIII), project RTI2018-100910-B-C41 (MCUI/

AEI/FEDER, UE), and the Generalitat Valenciana (PROMETEO/2018/024). IG-C was funded by Generalitat Valenciana (ACIF/2016/030). L.P. was funded by Ministerio de Economia, Industria y Competitividad (FPI grant). S.S. was funded by Instituto de Salud Carlos III and the European Social Fund "Sara Borrell" (CD16/000237). J.M.C. was funded by Sociedad Española de Oncología Médi-ca (Río Hortega-SEOM).

Notes

The authors declare no competing financial interest.

■ ACKNOWLEDGMENTS

The authors would like to thank the INCLIVA Biobank (PT17/0015/0049; B.000768 ISCIII) and the Valencian Biobanking Network integrated into the Spanish National Biobanks Network for providing the human biological samples. We would also like to thank the plasma donors and the nursing staff that accepted to participate in this study.

■ ABBREVIATIONS USED

BC, breast cancer; miRNAs, microRNAs; qRT-PCR, quantitative real-time polymerase chain reaction; NAA, nanoporous anodic alumina; FESEM, field emission scanning electron microscopy; EDX, energy-dispersive X-ray spectroscopy; APTES, (3-aminopropyl)triethoxysilane; TRIS, tris-(hydroxymethyl)aminomethane; ACN, acetonitrile; ROC, receiver-operating characteristics; AUC, area under curve; LOD, limit of detection

■ REFERENCES

(1) Bray, F.; Ferlay, J.; Soerjomataram, I.; Siegel, R. L.; Torre, L. A.; Jemal, A. Global cancer statistics 2018: GLOBOCAN estimates of incidence and mortality worldwide for 36 cancers in 185 countries. *Ca-Cancer J. Clin.* **2018**, *68*, 394−424.

(2) Miller, K. D.; Nogueira, L.; Mariotto, A. B.; Rowland, J. H.; Yabroff, K. R.; Alfano, C. M.; Jemal, A.; Kramer, J. L.; Siegel, R. L. Cancer treatment and survivorship statistics, 2019. *Ca-Cancer J. Clin.* **2019**, *69*, 363−385.

(3) Jafari, S. H.; Saadatpour, Z.; Salmaninejad, A.; Momeni, F.; Mokhtari, M.; Nahand, J. S.; Rahmati, M.; Mirzaei, H.; Kianmehr, M. Breast cancer diagnosis: Imaging techniques and biochemical markers. *J. Cell. Physiol.* **2018**, *233*, 5200−5213.

(4) Kashyap, D.; Kaur, H. Cell-free miRNAs as non-invasive biomarkers in breast cancer: Significance in early diagnosis and metastasis prediction. *Life Sci.* **2020**, *246*, No. 117417.

(5) Ng, E. K. O.; Li, R.; Shin, V. Y.; Jin, H. C.; Leung, C. P. H.; Ma, E. S. K.; Pang, R.; Chua, D.; Chu, K.- M.; Law, W. L.; et al. Circulating microRNAs as Specific Biomarkers for Breast Cancer Detection. *PLoS One* **2013**, *8*, No. e53141.

(6) Loh, H.-Y.; Norman, B. P.; Lai, K.-S.; Rahman, N. M. A. N. A.; Alitheen, N. B. M.; Osman, M. A. The regulatory role of microRNAs in breast cancer. *Int. J. Mol. Sci.* **2019**, *20*, No. 4940.

(7) Cortez, M. A.; Welsh, J. J.; Calin, G. A. Circulating MicroRNAs as Noninvasive Biomarkers in Breast Cancer. *Recent Results Cancer Res.* **2012**, *195*, 151−161.

(8) Bartel, D. P. MicroRNAs: Genomics, Biogenesis, Mechanism, and Function. *Cell* **2004**, *116*, 281−297.

(9) Kent, O. A.; Mendell, J. T. A small piece in the cancer puzzle: microRNAs as tumor suppressors and oncogenes. *Oncogene* **2006**, *25*, 6188−6196.

(10) Tormo, E.; Ballester, S.; Adam-Artigues, A.; Burgués, O.; Alonso, E.; Bermejo, B.; Menéndez, S.; Zazo, S.; Madoz-Gúrpide, J.; Rovira, A.; et al. The miRNA-449 family mediates doxorubicin resistance in triple-negative breast cancer by regulating cell cycle factors. *Sci. Rep.* **2019**, *9*, No. 5316.

(11) Tormo, E.; Adam-Artigues, A.; Ballester, S.; Pineda, B.; Zazo, S.; González-Alonso, P.; Albanell, J.; Rovira, A.; Rojo, F.; Lluch, A.; et al. The role of miR-26a and miR-30b in HER2+ breast cancer trastuzumab resistance and regulation of the CCNE2 gene. *Sci. Rep.* **2017**, *7*, No. 41309.

(12) van Schooneveld, E.; Wouters, M. C. A.; Van der Auwera, I.; Peeters, D. J.; Wildiers, H.; Van Dam, P. A.; Vergote, I.; Vermeulen, P. B.; Dirix, L. Y.; Van Laere, S. J. Expression profiling of cancerous and normal breast tissues identifies microRNAs that are differentially expressed in serum from patients with (metastatic) breast cancer and healthy volunteers. *Breast Cancer Res.* **2012**, *14*, No. R34.

(13) Matamala, N.; Vargas, M. T.; González-Cámpora, R.; Miñambres, R.; Arias, J.; Menéndez, P.; Andrés-León, E.; Mez-López, G. G.; Yanowsky, K.; Calvete-Candenas, J.; et al. Tumor MicroRNA expression profiling identifies circulating MicroRNAs for early breast cancer detection. *Clin. Chem.* **2015**, *61*, 1098−1106.

(14) Chen, Y.; Santos, A.; Wang, Y.; Kumeria, T.; Li, J.; Wang, C.; Losic, D. Biomimetic Nanoporous Anodic Alumina Distributed Bragg Reflectors in the Form of Films and Microsized Particles for Sensing Applications. *ACS Appl. Mater. Interfaces* **2015**, *7*, 19816−19824.

(15) Hofmann, C.; Duerkop, A.; Baeumner, A. J. Nanocontainers for Analytical Applications. *Angew. Chem., Int. Ed.* **2019**, *58*, 12840−12860.

(16) García-Fernández, A.; Aznar, E.; Martínez-Máñez, R.; Sancenón, F. New Advances in In Vivo Applications of Gated Mesoporous Silica as Drug Delivery Nanocarriers. *Small* **2020**, *16*, No. 1902242.

(17) Aznar, E.; Oroval, M.; Pascual, L.; Murguía, J. R.; Martínez-Máñez, R.; Sancenón, F. Gated Materials for On-Command Release of Guest Molecules. *Chem. Rev.* **2016**, *116*, 561−718.

(18) Ribes, À.; Xifré-Pérez, E.; Aznar, E.; Sancenón, F.; Pardo, T.; Marsal, L. F.; Martínez-Máñez, R. Molecular gated nanoporous anodic alumina for the detection of cocaine. *Sci. Rep.* **2016**, *6*, No. 38649.

(19) Ribes, À.; Aznar, E.; Santiago-Felipe, S.; Xifre-Perez, E.; Tormo-Mas, M. Á.; Pemán, J.; Marsal, L. F.; Martínez-Mántildez, R. Selective and Sensitive Probe Based in Oligonucleotide-Capped Nanoporous Alumina for the Rapid Screening of Infection Produced by *Candida albicans*. *ACS Sens.* **2019**, *4*, 1291−1298.

(20) Pla, L.; Santiago-Felipe, S.; Tormo-Más, M. Á.; Pemán, J.; Sancenón, F.; Aznar, E.; Martínez-Máñez, R. Aptamer-Capped Nanoporous Anodic Alumina for *Staphylococcus aureus* Detection. *Sens. Actuators, B* **2020**, *320*, No. 128281.

(21) Pla, L.; Xifré-Pérez, E.; Ribes, À.; Aznar, E.; Marcos, M. D.; Marsal, L. F.; Martínez-Máñez, R.; Sancenón, F. A Mycoplasma Genomic DNA Probe using Gated Nanoporous Anodic Alumina. *ChemPlusChem* **2017**, *82*, 337−341.

(22) Sancenón, F.; Pascual, L.; Oroval, M.; Aznar, E.; Martínez-Máñez, R. Gated Silica Mesoporous Materials in Sensing Applications. *ChemistryOpen* **2015**, *4*, 418−437.

(23) Llopis-Lorente, A.; Lozano-Torres, B.; Bernardos, A.; Martínez-Máñez, R.; Sancenón, F. Mesoporous silica materials for controlled delivery based on enzymes. *J. Mater. Chem. B* **2017**, *5*, 3069−3083.

(24) Oroval, M.; Coll, C.; Bernardos, A.; Marcos, M. D.; Martínez-Máñez, R.; Shchukin, D. G.; Sancenón, F. Selective Fluorogenic Sensing of As(III) Using Aptamer-Capped Nanomaterials. *ACS Appl. Mater. Interfaces* **2017**, *9*, 11332−11336.

(25) Garrido-Cano, I.; Constâncio, V.; Adam-Artigues, A.; Lameirinhas, A.; Simón, S.; Ortega, B.; Martínez, M. T.; Hernando, C.; Bermejo, B.; Lluch, A.; et al. Circulating miR-99a-5p Expression in Plasma: A Potential Biomarker for Early Diagnosis of Breast Cancer. *Int. J. Mol. Sci.* **2020**, *21*, No. 7427.

(26) Ragan, C.; Zuker, M.; Ragan, M. A. Quantitative prediction of miRNA-mRNA interaction based on equilibrium concentrations. *PLoS Comput. Biol.* **2011**, *7*, No. e1001090.

(27) Qavi, A. J.; Bailey, R. C. Multiplexed detection and label-free quantitation of microRNAs using arrays of silicon photonic microring resonators. *Angew. Chem., Int. Ed.* **2010**, *49*, 4608−4611.

(28) Yang, S. W.; Vosch, T. Rapid detection of microRNA by a silver nanocluster DNA probe. *Anal. Chem.* **2011**, *83*, 6935−6939.

https://dx.doi.org/10.1021/acssensors.0c02222
ACS Sens. 2021, 6, 1022−1029

(29) Hizir, M. S.; Balcioglu, M.; Rana, M.; Robertson, N. M.; Yigit, M. V. Simultaneous detection of circulating oncomiRs from body fluids for prostate cancer staging using nanographene oxide. *ACS Appl. Mater. Interfaces* **2014**, *6*, 14772−14778.
(30) Li, Y.; Liang, L.; Zhang, C. Y. Isothermally sensitive detection of serum circulating mirnas for lung cancer diagnosis. *Anal. Chem.* **2013**, *85*, 11174−11179.
(31) Youden, W. J. Index for rating diagnostic tests. *Cancer* **1950**, *3*, 32−35.
(32) Schisterman, E. F.; Perkins, N. J.; Liu, A.; Bondell, H. Optimal cut-point and its corresponding Youden index to discriminate individuals using pooled blood samples. *Epidemiology* **2005**, *16*, 73−81.

https://dx.doi.org/10.1021/acssensors.0c02222
ACS Sens. 2021, 6, 1022−1029